

White paper:

Biomax NICARA™ integrates structural brain connectomics

Abstract

We present NICARA™, a game-changing novel software enabling NeuroImaging-based Connectome Assessments for Research and Applications, on a knowledge-based semantic network platform. NICARA offers fully automated multi-modal imaging research for all medical doctors, psychiatrists and researchers via cloud in one step. The intelligent semantic integration algorithm empowers advanced statistical analysis to be possible with few mouse clicks.

Introduction

Medical brain Magnetic Resonance Imaging (MRI) analysis discovers more valuable information beyond visual inspection. It thus serves as a reliable knowledge base to develop new biomarkers so as to improve diagnosis and prognosis of brain diseases. However, the high complexity of scientific medical brain imaging analyses and relevant technical knowledge of hardware and software become barriers for frontier physicians to explore their scientific ideas. Many imaging approaches have been boosted by the development of dedicated imaging analysis technology, which can process not only 3 and 4-dimensional imaging data but also multi-modal brain images acquired by different imaging acquisition technologies. In the meantime, many research-orient imaging analysis tools have been developed by the academic community world-wide and were often released as open source. Nevertheless, scientific research achievement relies on reliable software and toolboxes, which should be maintained systematically to ensure high consistency and tangibility. Frequently, open source imaging analysis software users have to readapt deprecated functions or elements in their functioning pipelines after major updates.

NICARA is a cloud-based brain imaging analysis solution dedicated to structural connectome analysis, digitized integration and visualization. It is designed to integrate the core technologies established by peer reviewed scientific research, validated theoretical and technical integration methods, and verified data processing pipelines that are suitable for big data and cloud-based high-performance computing (HPC) as well as cloud storage. The fundamental pipelines used by NICARA have been optimized within the product servers of Biomax to ensure performance efficiency. In this way, NICARA can accomplish high quality HCP (Human Connectome Project; Van Essen et al., 2013) structural connectome analysis within a day, in contrast to 3 or more folds of processing duration using other systems.

In this paper, we first introduce the main concepts of the design and integration of NICARA. Second, we describe the software architecture, brain imaging connectome related tools, data and project management tools. Last but not least, we document use cases to demonstrate the major functionalities of NICARA in Real-World Data (RWD), which include NICARA processed connectomes and visualization files of HCP1200, the Alzheimer's Disease Neuroimaging Initiative (ADNI3; Weiner et al., 2017), and brain tumor study by Ghent University Hospital, Belgium (Aerts et al., 2018). These processed public data sets are ready for group-wise cross-sectional and longitudinal data analysis.

MRI Acquisition Guidance

We intend to encourage researchers to adapt then apply MR acquisition protocols of HCP in order to better exert the functionality of NICARA and ensure the processing outcome (<http://protocols.humanconnectome.org/>). An example clinic routine used by a Philips Achieva 3T scanner is included to demonstrate the detailed parameters to acquire high quality structural images within 30 minutes ('NICARA → CONNECTOME BUILDER → Available Protocols: Clinical MR Acquisition Protocol').

Considering that the ideal dual phase-encoding (PE) DWI acquisition MR sequence is still not a standard approach in most of the hospitals and research institutes, advanced pipelines are optional as advanced mode of NICARA and will be released depending on users' demands.

Pipeline

The image processing pipeline in NICARA is developed to perform the fully automated whole-brain structural connectome analysis by the CONNECTOME BUILDER in one step. The input images are T1 weighted (T1w), diffusion weighted images (DWI) in Nifti format, bvec and bval files. The DICOM data format will be included in an upcoming release of NICARA to automatically select required input data. The NICARA pipeline for whole-brain tractography is shown in figure 1.

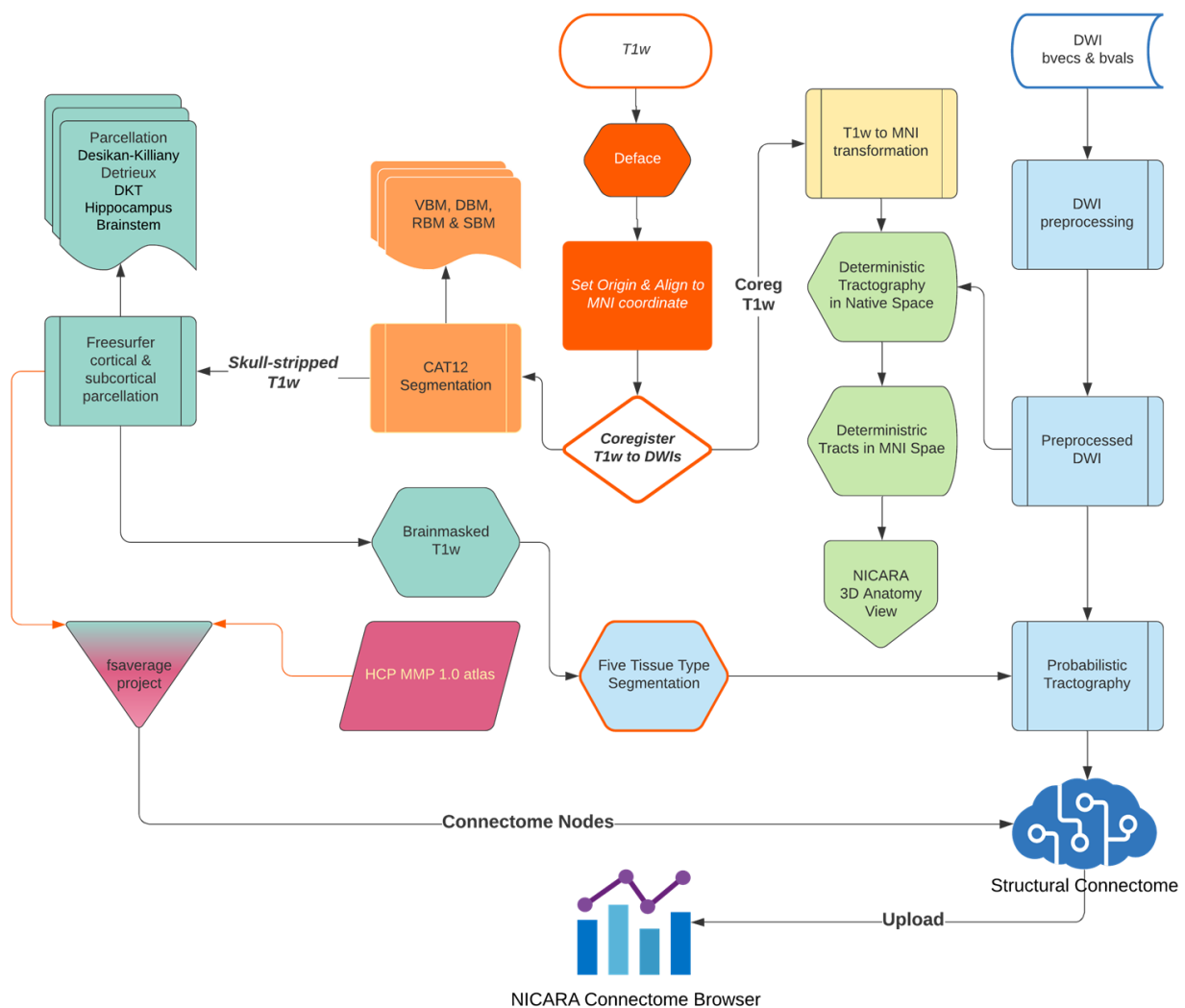


Figure 1. Overview of image processing pipeline in NICARA. T1w: T1 weighted image, DWI: diffusion weighted images, VBM: voxel-based morphometry, DBM: deformation-based morphometry, RBM: region-based morphometry, SBM: surface-based morphometry, DKT: Desikan-Killiany-Tourville atlas.

After all required files being uploaded to the CONNECTOME BUILDER, a click on 'Start DTI Tractography' initiates the pipeline confirmed by the dialog message:

"in processing

Retrieving data from NeuroXM...

Running DTI pipeline...

Importing results...

Running tracking...

Registering tractography data...

Running fiberselector...

Finished!

Generating files for visualization...

Finished!"

The total processing duration for an HCP subject is typically about 16 hours. The connectome results and data quality assessment can be viewed in the CONNECTOME BROWSER on-the-fly. The whole brain probabilistic tractography file (about 20 GB in tck format) is ready to download in zip format by a click.

Structural Image Processing

Preprocessing and Quality Assessment

The first step of the pipeline is to deface using the quickshear defacing method (Schimke & Hale, 2016). The raw images are removed immediately after the anonymization. Then we co-register the T1w image to the DWI image to ensure the brain parcellation and atlas ROI transformation precisely in the subject's native space. All defaced images are aligned to the origin and coordinate of the MNI template, i.e., MNI152 T1 template, which ensures the normalization and ROI creation later in the pipeline. The first output is the 'qc_registration.pdf' and an email notification is sent to the user. Users can verify the coregistration quality by clicking the 'QC image Registration' button in the 'General Information' page of the subject in the CONNECTOME BUILDER.

The second step segments the T1w image and performs morphometry analyses. The CAT12 toolbox (A Computational Anatomy Toolbox for SPM) in export mode is used to perform a tissue-based segmentation (Gaser et al., in review). The native T1w image is skull-stripped by the adaptive probability region-growing (APRG) approach, which refines the probability maps of the SPM approach by region-growing techniques of the 'gcut' approach with a final surface-based optimization strategy. This is currently the most accurate and reliable approach. That is why we directly input the skull-stripped T1w image to FreeSurfer (<https://surfer.nmr.mgh.harvard.edu/>; selected reference: Fischl et al., 2002; Fischl et al., 2004; Reuter et al., 2012) in the next step to perform whole brain parcellation and the HCP MMP 1.0 atlas projection. After skull-stripping, CAT12 segments the output T1w for voxel-based (VBM), deformation-based (DBM), region-based (RBM), and surface-based morphometry (SBM) approaches. Bias, noise and distortion correction are performed to improve segmentation quality. VBM uses the adaptive MAP approach for partial volume segmentation and the adaptation of local intensity changes to deal with varying tissue contrast (Dahnke et al. 2012a). DBM reveals information about the type and localization of structural differences between two brains, e.g., by Jacobian determinant. Therefore, DBM results can be used for subsequent analyses (Gaser et al., 1999). RBM maps different volume- and surface-based atlases to the individual brain by a high-dimensional spatial registration, then estimates the local tissue volumes inside the defined region of interest (ROI). ROI refers to an image mask of segmented brain regions predefined in an anatomical atlas, for instance the Automated Anatomical Labelling atlas 3 (AAL3, Rolls et al., 2020). Technically, ROI masks are labelled in arbitrary numbers so that each ROI can be extracted easily for further analysis. To precisely transform each ROI of the anatomical atlas from the MNI space to native space, the anatomical atlas has to be transformed to native space using inverse nonlinear deformations. SBM calculates the cortical thickness and reconstructs the central surface (Dahnke et al., 2013). Topological defects are repaired using spherical harmonics (Yotter et al., 2011a) and the cortical surface mesh is re-parameterized using area-distortion-reduced spherical maps (Yotter et al., 2011b).

The 'QC Image Segmentation' button in 'General Information' page reports detailed information of T1w image quality, segment volume, total intracranial volume (TIV) and averaged thickness with standard deviation. Image quality assessment measurements

include weighted average (IQR), image resolution, noise and bias. We consider 'bias' and 'weighted average' as gold standard over other parameters since they directly reflect the accuracy of segmentation. Grey matter (GM), white matter (WM) and cerebral spinal fluid (CSF) volumes are listed in absolute value (cm^3) as well as relative volume (%). TIV and GM thickness are important covariates for volumetric analyses of whole brain as well as brain regions, especially in the study of neurodegenerative diseases (Malone et al., 2015). All of these results are available for further approaches such as second level analysis and can be downloaded on demand.

Whole Brain Parcellation

The second main step of our pipeline is the FreeSurfer parcellation to create projected HCP MMP 1.0 atlas to native space for HCP connectome analysis (Fischl et al., 2004). The HCP MMP 1.0 atlas is the most detailed surface-based cortical atlas to date consisting of 360 ROIs in the cortex. And the structural connectome analysis provides network-based connectivity strength between ROIs throughout the brain by graph theory (Bonilha et al., 2015; Hagmann et al., 2008). To cover regions that are not included in the HCP MMP 1.0 atlas, we also implemented 19 regions of the Harvard-Oxford subcortical atlas (bilateral Cerebellum, Thalamus, Caudate, Putamen, Pallidum, Hippocampus, Amygdala, Accumbens, VentralDC, and Brain-Stem) in NICARA to parcellate subcortical areas (Desikan et al., 2006; Frazier et al., 2005; Goldstein et al., 2007; Makris et al., 2006). At the end of the FreeSurfer processing, the surface-based HCP MMP 1.0 atlas is transformed and projected to native space via 'fsaverage' image templates of FreeSurfer. In the NICARA pipeline, the classic 'recon-all' plus 'brainstem' and 'hippocampus subfields' processing is performed on the skull-stripped T1w image output from the CAT12 segmentation (Iglesias, Augustinack, et al., 2015; Iglesias, Van Leemput, et al., 2015). This further ensures the FreeSurfer parcellation success rate when processing low quality T1w images. As a result, cortical, subcortical, brainstem subfield and hippocampus subfield parcellations are processed with FreeSurfer built-in atlases.

FreeSurfer parcellation in the pipeline of NICARA provides 3 built-in classic brain atlases widely used in imaging research: Destrieux Atlas (Destrieux et al., 2010; Fischl et al., 2004), Desikan-Killiany Atlas (Desikan et al., 2006), and DKT Atlas (Desikan–Killiany–Tourville, <http://mindboggle.info/data.html>; Klein & Tourville, 2012). This results in up to 836 (HCP MMP 1.0: 360 ROIs + Harvard-Oxford subcortical atlas: 19 ROIs + FreeSurfer atlases: 457 ROIs) parcellated brain regions available in NICARA for further study. This forms a firm foundation to fulfill varied requirements from neurosurgeons to research scientists. In the near future, further and more specific atlases will be added to NICARA.

Diffusion Weighted Image Processing and Tractography Based Connectome Analysis

Step 3 focuses on the DWI data preprocessing, whole brain probabilistic tractography and surface based structural connectome analysis. In short, we applied Anatomically-Constrained Tractography (ACT) recommended by mrtrix3 (Tournier et al., 2019) for HCP comparable data quality and HCP connectome analysis (Smith et al., 2012). In DWI pre-processing, multiple forms of image noise and distortion, i.e., motion, unringing, eddy current and inhomogeneity etc., are corrected by performing a delicate sequence of steps using optimized tools such as mrtrix3, FSL6.0.2 (FMRIB Software Library; Jenkinson et al., 2012) and ANTs (Advanced Normalization Tools, <http://stnava.github.io/ANTs/>; Avants et al., 2014).

To perform ACT, the T1w image is segmented into a ‘five-tissue-type (5TT)’ format 4D image. These five 3D volumes are composed in a fixed order so that the anatomical priors will be applied accordingly during tractography. The ordered image volumes are: 1. Cortical grey matter, 2. Subcortical grey matter, 3. White matter, 4. CSF, 5. Pathological tissue. The pathological tissue can be brain regions that contain unknown architecture of the tissue, e.g., tumor, therefore no anatomical priors can be applied. For any streamline entering such a region, no anatomical priors are applied until the streamline either exists from that region, or stops due to some other streamline termination criteria. This image is specifically meaningful for neurosurgeons or clinicians who are working with patients with brain

damages or abnormalities. Options such as manually delineating tissue architecture of those brain regions can be added depending on the demands of advanced users.

Multi-Shell Multi-Tissue Constrained Spherical Deconvolution (MSMT-CSD) exploits the unique b-value dependencies of the different macroscopic tissue types (WM/GM/CSF) to estimate a multi-tissue orientation distribution function (ODF; Jeurissen et al., 2014). As it includes separate compartments for each tissue type, it can produce a map of the WM/GM/CSF signal contributions directly from the DW data. In addition, the more complete modeling of the DW signal results in more accurate apparent fiber density (AFD) measures and more precise fiber orientation estimates at the tissue interfaces.

The initial tractogram is generated by applying MSMT-CSD with a maximal fiber length of 250 mm and cutoff threshold of 0.06, following the recommendations of mtrix3 for the HCP project. The Spherical-deconvolution Informed Filtering of Tractograms (SIFT/SIFT2) algorithm provides more biologically meaningful estimates of structural connection density, although SIFT/SIFT2 reduces the overall streamline count (Smith et al., 2013, 2015). It will be an option of advanced features for expert mode depending on the users' demands. This feature alone increases about 50% of computation load on our HPC system and significantly prolongs the total processing time. Therefore, this function is currently excluded in this release of NICARA.

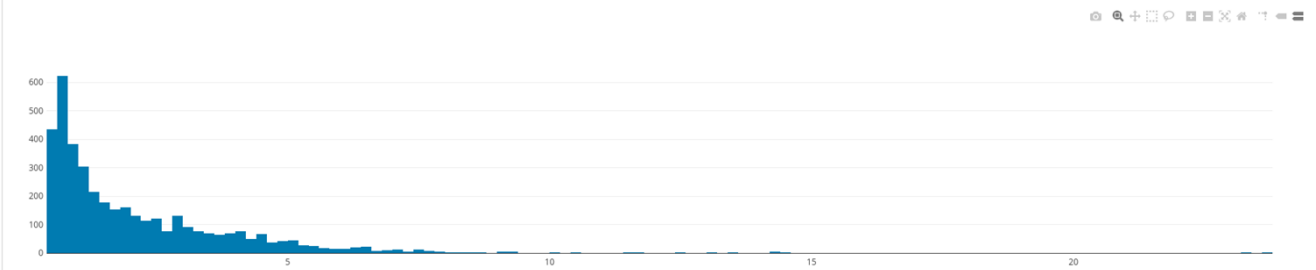
Probabilistic tractography employs ACT as default while SIFT serves as an advanced feature on demand. Then, reconstructed streamlines are mapped to the parcellated image, e.g., the HCP MMP 1.0 atlas parcellated ROI map transformed into native space, to produce a connectome. An HCP-connectome computed by NICARA obtains a 379 x 379 matrix, which typically results in about 100,000 valid connections all over the brain. The final results are uploaded to NICARA by a csv-file, which can be viewed by clicking the 'Tabular Listing' button after connectome import processing is accomplished (Fig.2).

CONNECTOME BROWSER

Subject: 183741 | Longitudinal Assessment: Day 0 | Cohort: Control | Study: HCP Young Adult

DTI 3D Lattice Threshold (≥ 0.5)
 fMRI 3D Anatomy Subnetwork
 MEG Tabular Listing Seed

Histogram and tabular view of connections in DTI Tractography 127_5_6433_DTI 1 of 158 | Per page: 25 | Results: 3,944



Filter results by:

Selected items: 0 Show/Hide | Sort by

Origin	Target			Fiber Density Absolute	Fiber Density Normalized				
Region of Interest	X	Y	Z	Region of Interest	X	Y	Z		
<input type="checkbox"/> L_V1	-5.0	-89.0	0.0	<input checked="" type="checkbox"/> L_V6	-15.0	-75.0	21.0	1.56846517237864	0.066188575588098
<input type="checkbox"/> L_V1	-5.0	-89.0	0.0	<input checked="" type="checkbox"/> L_V2	-22.0	-102.0	7.0	23.6969168537398	1.0
<input type="checkbox"/> L_V1	-5.0	-89.0	0.0	<input checked="" type="checkbox"/> L_V3	-23.0	-95.0	10.0	8.61362974345684	0.363491579795852
<input type="checkbox"/> L_V1	-5.0	-89.0	0.0	<input checked="" type="checkbox"/> L_V4	-32.0	-93.0	9.0	3.09198100092181	0.130480307628452
<input type="checkbox"/> L_V1	-5.0	-89.0	0.0	<input checked="" type="checkbox"/> L_V3A	-18.0	-88.0	19.0	2.87020209078037	0.121121330192261
<input type="checkbox"/> L_V1	-5.0	-89.0	0.0	<input checked="" type="checkbox"/> L_Pro5	-18.0	-51.0	3.0	1.63422128214734	0.068963455973363

Figure 2. The 'Tabular Listing' view of an example HCP young adult subject in the CONNECTOME BROWSER. This figure shows about 3000 connections only, which are greater or equal to the set-point.

3D Anatomy Visualization

The structural connectome results are presented in a 3D lattice viewer in the CONNECTOME BROWSER (Fig.3). All valid connections between ROIs predefined by the HCP MMP 1.0 and Harvard-Oxford subcortical atlas cover the whole brain network. Absolute fiber density is defined as the contribution of the total number of streamlines to the connectome edge scaled by the inverse of two node volumes. Normalized fiber density is the regulated value in a range between maximal and minimal absolute fiber density. Strong connections (absolute fiber density) between 2 nodes (sphere in centroid coordinate of a segmented brain region) are revealed in thick lines whereas weak connections are shown in thin lines. In total, about three to five thousand valid connections (threshold ≥ 1.0 by default) of an HCP young adult are superimposed on a high-resolution transparent glass-brain template in MNI space.

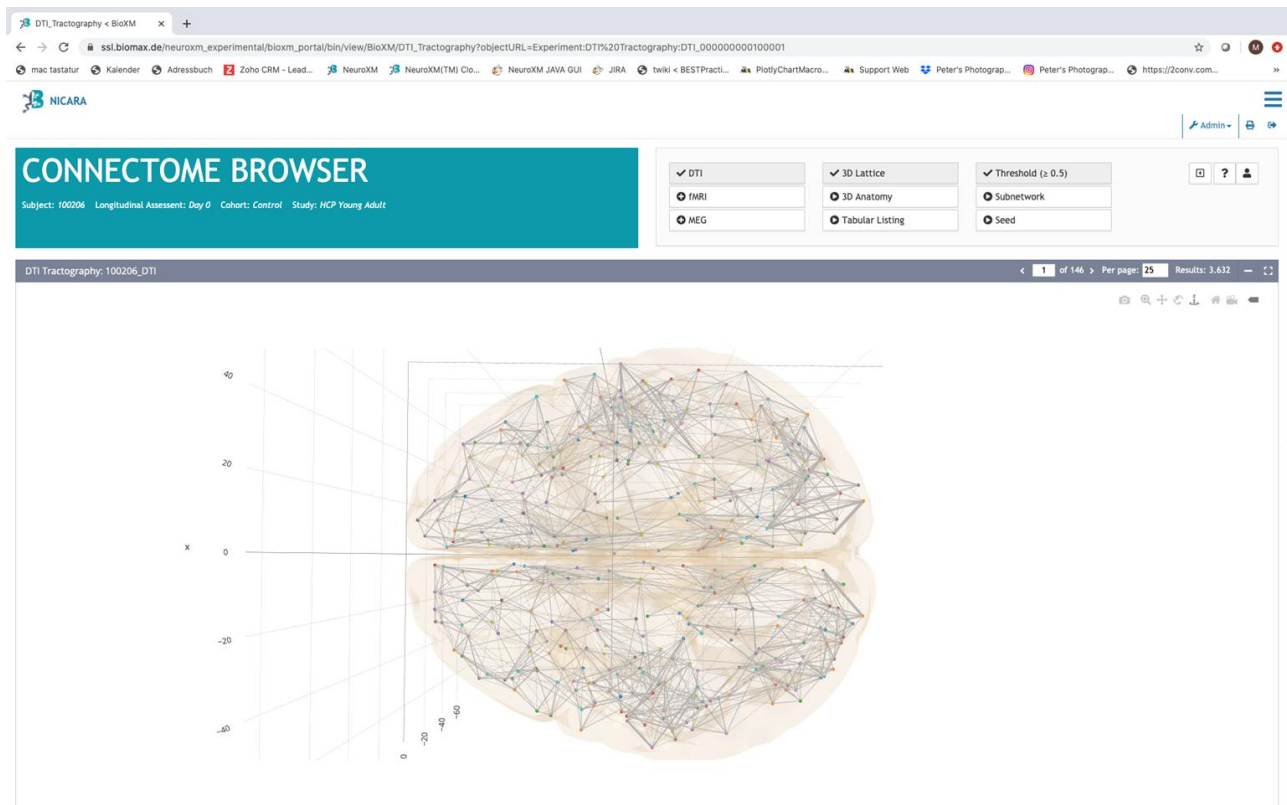


Figure 3. The 3D lattice view of an example HCP young adult subject in the CONNECTOME BROWSER.

The 3D Anatomy viewer, a Biomax customized version of BrainGL Web (Max Planck Institute for Human Cognitive and Brain Science, Leipzig), includes 2 view modes: 3D Anatomy (Native) and 3D Anatomy (MNI). The MNI mode shows deterministic tractography of the processed subject by clicking the '3D Anatomy' button on the connectome viewer page. In total, 9 predefined fiber bundles are presented in a 1 mm T1w image in MNI space (Fig.4A). The reconstructed fibers are Cingulum, Frontal Aslant Tract, Homotopic Contralateral Connections, Inferior Fronto-Occipital Fasciculus, Inferior Longitudinal Fasciculus, Middle Longitudinal Fasciculus, Superior Longitudinal Fasciculus, Uncinate Fasciculus, and Vertical Occipital Fasciculus. Users can view the fibers by selecting one or more check-boxes at the up-right side of the viewer on-the-fly. The 'Select all' and 'Unselect all' buttons allow users to view or clear all fiber bundles. Three color modes, i.e., Default, Local and Global, are available to label fiber bundles. In 'Default' color mode, each fiber bundle is labelled by an arbitrary color to achieve visual distinction. In 'Local' color mode, fibers are labelled in red, green and blue color, where red represents fiber orientation in left-right, while green represents fiber in anterior-posterior orientation, and blue represents fiber

in superior-inferior orientation following the Directionally Encoded Color scheme (DEC; Pajevic & Pierpaoli, 1999; Fig.4E). In 'Global' mode, the red, green and blue color-coding represent the orientation of the vector between starting and ending points of a fiber following the same theory as 'Local' mode.

Three atlas modes, i.e. HCP MMP 1.0 Map, HCP MMP 1.0 Volumes, and JHU WM (JHU white-matter tractography atlas, Johns Hopkins University; Mori et al., 2005), are available in 'Select Atlas' menu to verify reconstructed fibers according to anatomical landmarks in the 3D Anatomy view. In the 'HCP MMP 1.0 Map' mode (Fig.4A), 360 color-coded regions are superimposed over the T1 MNI image so that users can view each fiber pathway along with anatomical landmarks. In 'HCP MMP 1.0 Volumes' mode, transparent 3D shape images of 'seed' and 'end' ROIs of each predefined fiber are superimposed over the T1w image, which allows users to vividly view the actual anatomical representation of how reconstructed fibers connect anatomical regions segmented based on HCP MMP 1.0 atlas (Fig.4B&C). All 3D shape ROI images are well balanced for color, rendering and transparency, therefore it maximizes visibility of all detailed information on-the-fly.

The 3D anatomy plot can be rotated in 3D (holding the left mouse button), zoomed in/out (middle mouse roll forwards/backwards scrolling), and moved in 2D (holding the middle mouse button then drag to move). A color-coded 3D cube dynamically represents the rotation of the anatomy plot in 3D space. Capital letter on each surface of the cube indicates the anterior (A) or posterior (P) side in coronal view, left (L) or right (R) side in sagittal view, and inferior (I) or superior (S) part in axial view. The edges are colored following the DEC scheme to indicate fiber directions (Pajevic & Pierpaoli, 1999, Fig.4E). The 'Set view' menu is placed below the 'Color mode' to select Coronal, Sagittal, Axial as well as Reset to default view. Image slice sliders in three anatomical planes and a button to reset the origin of the image ('Center Slices') are placed below 'Color mode' menu. Left sliding the handle in x axis moves sagittal slice left, in y axis pushes coronal slice posterior, and in z axis brings axial slice inferior; whereas right sliding the knob evokes the reversed slice sliding accordingly.

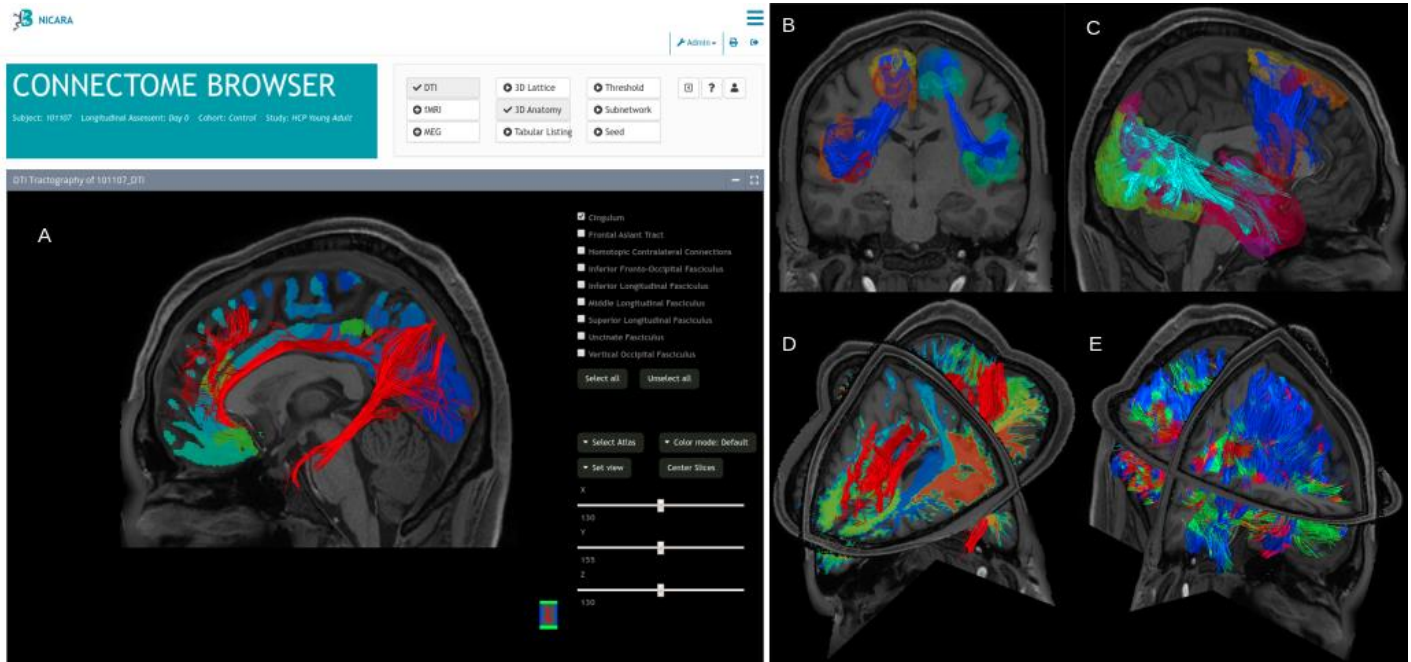


Figure 4. 3D anatomic view of predefined fiber tracts in NICARA. A. The fiber tracts of the Cingulum of an example HCP young adult are presented in 'default' color mode in sagittal plane together with the HCP MMP 1.0 color-coded atlas superimposed on the T1w template in MNI space. B. Bilateral Frontal Aslant Tracts are viewed in 'default' color mode superimposed by 'seed' and 'end' ROIs extracted from the HCP MMP 1.0 atlas. C. Sagittal view of Frontal Aslant Tract and Inferior Longitudinal Fasciculus with same view settings as B. D. Cingulum tracts are superimposed on the color-coded JHU white-matter tractography atlas. E. An overview of all 9 predefined tracts is presented in 'local' DEC color mode.

Statistic Model Design and Specification

The CONNECTOME EDITOR creates and stores subnetworks of the connectome. Major fiber tracts (9), functional (8) and brain region subnetworks (36) are predefined for users to explore their connectomes for general analyses. The major fiber tract subnetworks employ the same ROI definition of the nine major fiber tracts used for the tractography visualization. The functional subnetworks are Auditory, Default Mode, Dorsal Attention, Salience, Semantic Language, Supplementary Motor, Ventral Attention, and Ventral Premotor Network defined by resting state functional MRI (Fox & Raichle, 2007; Briggs et al., 2018; Fig.5). Each subnetwork uses all validated connectivity nodes of the connectome in the subnetwork for further statistical comparisons. The brain region subnetworks are adapted from HCP MMP 1.0 atlas and restricted by anatomical priors.

Subnetworks can be easily created by users' definition and stored for further analyses (Briggs et al., 2018). In this way, the CONNECTOME EDITOR automatically offers unlimited subnetwork options for users to explore their connectomes.

The CONNECTOME COMPARATOR makes comparisons between connectomes. Connectome comparisons are available at individual and group level. At the individual level, connectome comparisons between a patient versus the matched control are created by 'Create Patient Report'. Similarly, longitudinal differences of a patient between 2 time points can be assessed by 'Evaluate Longitudinal Changes'. At the group level, users define 2 groups to be compared by 'Create Group Comparison' under a predefined or user-chosen subnetwork. 'Check Connectivity Variability' reveals the connectivity variability of a user-defined age range in the HCP Young Adult Study subjects.

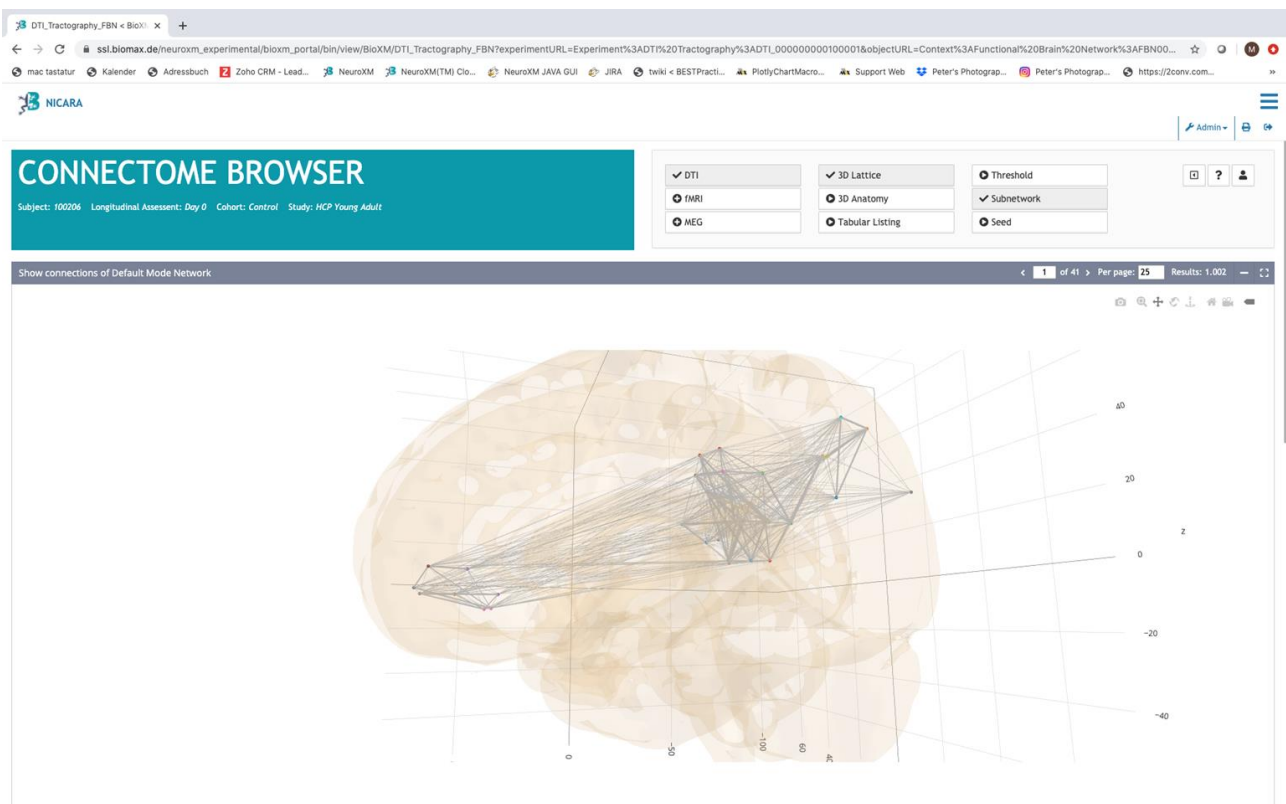


Figure 5. The default mode network of an example HCP young adult subject is presented in 3D lattice view of the CONNECTOME BROWSER.

Processed Public Data Sets

NICARA processed 1065 subjects of the HCP1200 young adult study and stored their connectomes in the cloud. Ten Alzheimer's disease patients versus ten mild cognitive impairment patients versus ten matched control subjects of the Alzheimer's Disease Neuroimaging Initiative 3 (ADNI3) project were also processed to exemplify a use case of degenerative brain disease by NICARA. 25 human brain tumor patients and 11 human control participants of Ghent University Hospital, Belgium, were analyzed to stretch the robustness of NICARA. More public data sets are possible to be included as users' demand.

Conclusion

We introduce NICARA by Biomax, a cloud-based software for NeuroImaging-based Connectome Assessments in Research and Application. The CONNECTOME BUILDER employs a sophisticated pipeline integrating broadly used main-stream image processing analysis software and tools, and accomplishes complex brain imaging analyses with only a few mouse clicks. The CONNECTOME EDITOR and COMPARATOR are designed to easily perform group-wise inter- and intra-subnetwork comparison analyses. The CONNECTOME BROWSER provides an overview and general information of project, study and subjects. NICARA is an intuitive, reliable, and efficient assistant for medical doctors and researchers to spread their ideas from high quality imaging research to a broader scientific research community.

Acknowledgment

Data were provided [in part] by the Human Connectome Project, WU-Minn Consortium (Principal Investigators: David Van Essen and Kamil Ugurbil; 1U54MH091657) funded by the 16 NIH Institutes and Centers that support the NIH Blueprint for Neuroscience Research; and by the McDonnell Center for Systems Neuroscience at Washington University.

References

- Avants, B. B., Tustison, N. J., Stauffer, M., Song, G., Wu, B., & Gee, J. C. (2014). The Insight ToolKit image registration framework. *Frontiers in neuroinformatics*, 8, 44. <https://doi.org/10.3389/fninf.2014.00044>
- Aerts, H., Schirner, M., Jeurissen, B., Van Roost, D., Achten, E., Ritter, P., & Marinazzo, D. (2018). Modeling Brain Dynamics in Brain Tumor Patients Using the Virtual Brain. *Eneuro*, 5(3), ENEURO.0083-18.2018. <https://doi.org/10.1523/ENEURO.0083-18.2018>
- Bonilha, L., Gleichgerrcht, E., Fridriksson, J., Breedlove, J. L., Rorden, C., Nesland, T., Paulus, W., Helms, G., & Focke, N. K. (2015). Reproducibility of the structural brain connectome derived from diffusion tensor imaging. *PLoS ONE*, 10(9). <https://doi.org/10.1371/journal.pone.0135247>
- Briggs RG, Conner AK, Baker CM, Burks JD, Glenn CA, Sali G, Battiste JD, O'Donoghue DL, Sughrue ME. A Connectomic Atlas of the Human Cerebrum-Chapter 18: The Connectional Anatomy of Human Brain Networks. *Oper Neurosurg (Hagerstown)*. 2018 Dec 1;15(suppl_1):S470-S480. doi: 10.1093/ons/opy272.
- Dahnke, R., Yotter, R. A., & Gaser, C. (2013). Cortical thickness and central surface estimation. *NeuroImage*, 65, 336–348. <https://doi.org/10.1016/j.neuroimage.2012.09.050>
- Desikan, R. S., Ségonne, F., Fischl, B., Quinn, B. T., Dickerson, B. C., Blacker, D., Buckner, R. L., Dale, A. M., Maguire, R. P., Hyman, B. T., Albert, M. S., & Killiany, R. J. (2006). An automated labeling system for subdividing the human cerebral cortex on MRI scans into gyral based regions of interest. *NeuroImage*, 31(3), 968–980. <https://doi.org/10.1016/j.neuroimage.2006.01.021>
- Destrieux, C., Fischl, B., Dale, A., & Halgren, E. (2010). Automatic parcellation of human cortical gyri and sulci using standard anatomical nomenclature. *NeuroImage*, 53(1), 1–15. <https://doi.org/10.1016/j.neuroimage.2010.06.010>
- Fischl, B., Van Der Kouwe, A., Destrieux, C., Halgren, E., Ségonne, F., Salat, D. H., Busa, E., Seidman, L. J., Goldstein, J., Kennedy, D., Caviness, V., Makris, N., Rosen, B., & Dale, A. M. (2004). Automatically Parcellating the Human Cerebral Cortex. *Cerebral Cortex*, 14(1), 11–22. <https://doi.org/10.1093/cercor/bhg087>
- Fox, M. D., & Raichle, M. E. (2007). Spontaneous fluctuations in brain activity observed with functional magnetic resonance imaging. In *Nature Reviews Neuroscience* (Vol. 8, Issue 9, pp. 700–711). Nature Publishing Group. <https://doi.org/10.1038/nrn2201>
- Frazier, J. A., Chiu, S., Breeze, J. L., Makris, N., Lange, N., Kennedy, D. N., Herbert, M. R., Bent, E. K., Koneru, V. K., Dieterich, M. E., Hodge, S. M., Rauch, S. L., Grant, P. E., Cohen, B. M., Seidman, L. J., Caviness, V. S., & Biederman, J. (2005). Structural brain magnetic resonance imaging of limbic and thalamic volumes in pediatric bipolar disorder. *American Journal of Psychiatry*, 162(7), 1256–1265. <https://doi.org/10.1176/appi.ajp.162.7.1256>

- Gaser, C., Volz, H. P., Kiebel, S., Riehemann, S., & Sauer, H. (1999). Detecting structural changes in whole brain based on nonlinear deformations application to schizophrenia research. *NeuroImage*, *10*(2), 107–113. <https://doi.org/10.1006/nimg.1999.0458>
- Goldstein, J. M., Seidman, L. J., Makris, N., Ahern, T., O'Brien, L. M., Caviness, V. S., Kennedy, D. N., Faraone, S. V., & Tsuang, M. T. (2007). Hypothalamic Abnormalities in Schizophrenia: Sex Effects and Genetic Vulnerability. *Biological Psychiatry*, *61*(8), 935–945. <https://doi.org/10.1016/j.biopsych.2006.06.027>
- Hagmann, P., Cammoun, L., Gigandet, X., Meuli, R., Honey, C. J., Wedeen, V. J., & Sporns, O. (2008). Mapping the Structural Core of Human Cerebral Cortex. *PLoS Biology*, *6*(7), e159. <https://doi.org/10.1371/journal.pbio.0060159>
- Iglesias, J. E., Augustinack, J. C., Nguyen, K., Player, C. M., Player, A., Wright, M., Roy, N., Frosch, M. P., McKee, A. C., Wald, L. L., Fischl, B., & Van Leemput, K. (2015). A computational atlas of the hippocampal formation using ex vivo, ultra-high resolution MRI: Application to adaptive segmentation of in vivo MRI. *NeuroImage*, *115*, 117–137. <https://doi.org/10.1016/j.neuroimage.2015.04.042>
- Iglesias, J. E., Van Leemput, K., Bhatt, P., Casillas, C., Dutt, S., Schuff, N., Truran-Sacrey, D., Boxer, A., & Fischl, B. (2015). Bayesian segmentation of brainstem structures in MRI. *NeuroImage*, *113*, 184–195. <https://doi.org/10.1016/j.neuroimage.2015.02.065>
- Jeurissen, B., Tournier, J. D., Dhollander, T., Connelly, A., & Sijbers, J. (2014). Multi-tissue constrained spherical deconvolution for improved analysis of multi-shell diffusion MRI data. *NeuroImage*, *103*, 411–426. <https://doi.org/10.1016/j.neuroimage.2014.07.061>
- Tournier, J. D., Smith, R., Raffelt, D., Tabbara, R., Dhollander, T., Pietsch, M., Christiaens, D., Jeurissen, B., Yeh, C. H., & Connelly, A. (2019). MRtrix3: A fast, flexible and open software framework for medical image processing and visualisation. *NeuroImage*, *202*, 116137. <https://doi.org/10.1016/j.neuroimage.2019.116137>
- Jenkinson, M., Beckmann, C. F., Behrens, T. E., Woolrich, M. W., & Smith, S. M. (2012). FSL. *NeuroImage*, *62*(2), 782–790. <https://doi.org/10.1016/j.neuroimage.2011.09.015>
- Klein, A., & Tourville, J. (2012). 101 labeled brain images and a consistent human cortical labeling protocol. *Frontiers in neuroscience*, *6*, 171. <https://doi.org/10.3389/fnins.2012.00171>
- Makris, N., Goldstein, J. M., Kennedy, D., Hodge, S. M., Caviness, V. S., Faraone, S. V., Tsuang, M. T., & Seidman, L. J. (2006). Decreased volume of left and total anterior insular lobule in schizophrenia. *Schizophrenia Research*, *83*(2–3), 155–171. <https://doi.org/10.1016/j.schres.2005.11.020>
- Malone, I. B., Leung, K. K., Clegg, S., Barnes, J., Whitwell, J. L., Ashburner, J., Fox, N. C., & Ridgway, G. R. (2015). Accurate automatic estimation of total intracranial volume: A nuisance variable with less nuisance. *NeuroImage*, *104*, 366–372. <https://doi.org/10.1016/j.neuroimage.2014.09.034>
- Mori, S., Wakana, S., van Zijl, P.C.M., Nagae-Poetscher, L.M. MRI Atlas of Human White Matter. Elsevier, Amsterdam, The Netherlands (2005). eBook ISBN: 9780080456164

- Pajevic, S., & Pierpaoli, C. (1999). Color schemes to represent the orientation of anisotropic tissues from diffusion tensor data: Application to white matter fiber tract mapping in the human brain. *Magnetic Resonance in Medicine*. [https://doi.org/10.1002/\(SICI\)1522-2594\(199909\)42:3<526::AID-MRM15>3.0.CO;2-J](https://doi.org/10.1002/(SICI)1522-2594(199909)42:3<526::AID-MRM15>3.0.CO;2-J)
- Reuter, M., Schmansky, N.J., Rosas, H.D., Fischl, B. 2012. Within-Subject Template Estimation for Unbiased Longitudinal Image Analysis. *Neuroimage* 61 (4), 1402-1418.
- Rolls, E. T., Huang, C. C., Lin, C. P., Feng, J., & Joliot, M. (2020). Automated anatomical labelling atlas 3. *NeuroImage*, 206. <https://doi.org/10.1016/j.neuroimage.2019.116189>
- Schimke, N., & Hale, J. (2016). Quickshear Defacing for Neuroimages. *Proceedings of the 2nd USENIX Conference on Health Security and Privacy*.
- Smith, R. E., Tournier, J. D., Calamante, F., & Connelly, A. (2012). Anatomically-constrained tractography: Improved diffusion MRI streamlines tractography through effective use of anatomical information. *NeuroImage*, 62(3), 1924–1938. <https://doi.org/10.1016/j.neuroimage.2012.06.005>
- Smith, R. E., Tournier, J. D., Calamante, F., & Connelly, A. (2013). SIFT: Spherical-deconvolution informed filtering of tractograms. *NeuroImage*, 67, 298–312. <https://doi.org/10.1016/j.neuroimage.2012.11.049>
- Smith, R. E., Tournier, J. D., Calamante, F., & Connelly, A. (2015). SIFT2: Enabling dense quantitative assessment of brain white matter connectivity using streamlines tractography. *NeuroImage*, 119, 338–351. <https://doi.org/10.1016/j.neuroimage.2015.06.092>
- Van Essen, D. C., Smith, S. M., Barch, D. M., Behrens, T. E. J., Yacoub, E., & Ugurbil, K. (2013). The WU-Minn Human Connectome Project: An overview. *NeuroImage*. <https://doi.org/10.1016/j.neuroimage.2013.05.041>
- Weiner, M. W., Veitch, D. P., Aisen, P. S., Beckett, L. A., Cairns, N. J., Green, R. C., Harvey, D., Jack, C. R., Jagust, W., Morris, J. C., Petersen, R. C., Salazar, J., Saykin, A. J., Shaw, L. M., Toga, A. W., & Trojanowski, J. Q. (2017). The Alzheimer's Disease Neuroimaging Initiative 3: Continued innovation for clinical trial improvement. In *Alzheimer's and Dementia* (Vol. 13, Issue 5, pp. 561–571). Elsevier Inc. <https://doi.org/10.1016/j.jalz.2016.10.006>
- Yotter, Rachel A., Thompson, P. M., & Gaser, C. (2011). Algorithms to Improve the Reparameterization of Spherical Mappings of Brain Surface Meshes. *Journal of Neuroimaging*, 21(2). <https://doi.org/10.1111/j.1552-6569.2010.00484.x>
- Yotter, Rachel Aine, Dahnke, R., Thompson, P. M., & Gaser, C. (2011). Topological correction of brain surface meshes using spherical harmonics. *Human Brain Mapping*, 32(7), 1109–1124. <https://doi.org/10.1002/hbm.21095>